photonics

MDPI

Article

Reconstructed Hybrid Optical OFDM-NOMA for Multiuser VLC Systems

Baolong Li [1], Jianfeng Shi [1,2] and Simeng Feng [3]*

[1] School of Electronic and Information Engineering, Nanjing University of Information Science and Technology, Nanjing 210044, China
[2] National Mobile Communications Research Laboratory, Southeast University, Nanjing 210096, China
[3] Key Laboratory of Dynamic Cognitive System of Electromagnetic Spectrum Space, Ministry of Industry and Information Technology, Nanjing University of Aeronautics and Astronautics, Nanjing 210016, China
* Correspondence: simeng-feng@nuaa.edu.cn

Abstract: Non-orthogonal multiple access (NOMA) is deemed to be a prospective multiple access technology of the next generation. However, in visible light communication (VLC), when advanced hybrid optical orthogonal frequency division multiplexing (O-OFDM), such as hybrid asymmetrically clipped O-OFDM (HACO-OFDM), is combined with NOMA, error propagation is induced, which degrades the system performance. Therefore, a novel reconstructed hybrid O-OFDM-NOMA (RHO-OFDM-NOMA) scheme is conceived in this paper. In order to eliminate the error propagation, the users in RHO-OFDM-NOMA opt for the ACO-OFDM or clipping-free O-OFDM signals according to their channel qualities, which are subsequently superimposed on pulse-amplitude-modulated discrete multitone (PAM-DMT) to yield the spectrum-efficient hybrid O-OFDM signal. Furthermore, a reconstruction process is designed to ensure the non-negativity. Compared with HACO-OFDM, the proposed RHO-OFDM can retain the error propagation in NOMA-VLC, whilst maintaining the superiorities of high spectral and power efficiency. It is demonstrated by simulation results that RHO-OFDM-NOMA can support a notably higher data rate than the NOMA schemes using conventional O-OFDM.

Keywords: visible light communication (VLC); non-orthogonal multiple access (NOMA); optical orthogonal frequency division multiplexing (O-OFDM)

Citation: Li, B.; Shi, J.; Feng, S. Reconstructed Hybrid Optical OFDM-NOMA for Multiuser VLC Systems. *Photonics* **2022**, *9*, 857. https://doi.org/10.3390/photonics9110857

Received: 29 August 2022
Accepted: 8 November 2022
Published: 13 November 2022

1. Introduction

Visible light communication (VLC) exploits light rays emitted by light-emitting diode (LED) to transmit data [1,2]. Acting as a burgeoning wireless communication technology, VLC possesses many remarkable advantages, including low cost, license-free optical spectrum, high-speed data transmission, no electromagnetic contamination, etc. Given these remarkable advantages, VLC has gained great attention from both academia and the industry. It has also been recognized as a potential technology of the sixth generation (6G) of wireless communication [3,4].

In wireless communications, the booming development of information technology has led to explosively increased mobile data and smart devices [5]. Therefore, how to significantly boost the data rate and enhance the ability of user connectivity has become an urgent problem of 6G communication, which is also one of the main ongoing research efforts of VLC. On the other hand, one of the main drawback lies in the low communication bandwidth of the existing commercial LEDs in VLC, which makes this urgent problem more challenging for VLC [6,7]. In order to tackle the problem, multiple access (MA) technology plays a significant role.

In conventional orthogonal MA (OMA) schemes, strict orthogonality in the time or frequency domains is required to eliminate the multiuser interference. However, due to this strict orthogonality of the supported users, the OMA schemes cannot accommodate

requirements of the explosively increased mobile data and smart devices well. Against this background, non-orthogonal MA (NOMA) has gained tremendous attention and is deemed to be a potential MA technology of the next generation. Superior to OMA, NOMA can serve the simultaneous communication of multiple users in the same time and frequency resource, and notably enhances spectral efficiency and ability of the user connectivity in comparison with OMA [8]. Therefore, NOMA has numerous applications in VLC, and is regarded as one of the research directions [7,9]. NOMA should be used in combination with modulation. Relying on high spectral efficiency, orthogonal frequency division multiplexing (OFDM) constitutes competitive modulation in VLC. Furthermore, more ambitious system performance can be expected by combing NOMA with OFDM, which constitutes the concept of OFDM-NOMA [10].

In VLC, a real and non-negative signal is required due to the intensity-modulated direct detection [11,12]. Therefore, a variety of optical OFDM (O-OFDM) strategies have been conceived for VLC. With the aid of frequency-domain Hermitian symmetry, a real O-OFDM signal can be produced. For the sake of the non-negativity, numerous strategies have been conceived. A simple strategy is direct-current-biased O-OFDM (DCO-OFDM), in which a direct-current bias is used [13]. However, DCO-OFDM has to employ a comparatively large DC bias to avert non-linear distortion, resulting in a poor performance in terms of power efficiency. To address it, asymmetrically clipped O-OFDM (ACO-OFDM) has been designed, which generates a unipolar signal through direct clip of the negative part [14,15]. The same philosophy has been extended to discrete multitone modulation (DMT), yielding pulse-amplitude-modulated DMT (PAM-DMT). Nevertheless, these O-OFDM schemes waste half of the subcarrier resources, thus leading to spectral inefficiency [16].

To address the problem of conventional O-OFDM, more advanced hybrid O-OFDM schemes have been conceived [17]. In VLC, hybrid ACO-OFDM (HACO-OFDM) is deemed to be one of the widely used hybrid schemes, which exploits an amalgam of the ACO-OFDM and PAM-DMT techniques [18]. To expound further, the time-domain ACO-OFDM and PAM-DMT signals occupying different subcarriers are transmitted in parallel through direct superimposition. An iterative receiver can be utilized in HACO-OFDM to successively detect the two signal components. Given that the clipping operation of ACO-OFDM induces the interference with PAM-DMT, additional operation of eliminating the clipping distortion is required before detecting the PAM-DMT signal [19]. Compared with conventional schemes, HACO-OFDM can achieve substantial improvement of the spectral efficiency, whist maintaining high power efficiency. Therefore, HACO-OFDM has been widely applied in various scenarios of VLC [20–22].

Recently, there have been several important contributions to OFDM-NOMA in VLC. In [23], the performance of a multiple-input multiple-output-based, multiuser VLC system using DCO-OFDM-NOMA was investigated. By using the real-time software reconfigurable technique, Shi et al. [24] demonstrated an OFDM-NOMA VLC system with dynamic resource allocation. Furthermore, an OFDM-NOMA VLC with the aid of offset quadrature amplitude modulation (QAM) was experimentally demonstrated in [25]. For the sake of the improvement in both user fairness and throughput, a resource allocation method was investigated for the OFDM-NOMA VLC in [26]. In [27], joint power allocation and user pairing was studied for ACO-OFDM-NOMA system to achieve massive connectivity and energy saving. However, these exciting works are mainly developed based on ACO-OFDM and DCO-OFDM, which suffer from spectral and power inefficiency, respectively. OFDM-NOMA using the more advanced hybrid O-OFDM has not been deeply investigated. Moreover, users with worse channel quality can only partially decode the transmitted symbols. Although, when the existing hybrid O-OFDM scheme is combined with NOMA, the clipping distortion elimination should depend on the transmitted symbols of all users. Therefore, error propagation can be induced for users with the worse channel, leading to performance degradation.

In the paper, a novel reconstructed hybrid O-OFDM-NOMA (RHO-OFDM-NOMA) is designed for VLC. In RHO-OFDM-NOMA, the ACO-OFDM and clipping-free O-OFDM

signals using the odd-indexed subcarrier for transmission are adopted for different NOMA users according to their channel quality in the proposed scheme to avoid error propagation. Furthermore, these O-OFDM signals are combined with PAM-DMT to yield the spectrum-efficient RHO-OFDM signal, which is subsequently made non-negative by introducing a reconstruction process. The novelty and contributions are summarized as follows:

1. The proposed RHO-OFDM exploits the simultaneous transmission of multiple O-OFDM signals, which effectively enhances the spectral efficiency compared with ACO-OFDM. Meanwhile, no direct-current bias is added in RHO-OFDM, thus leading to high power efficiency.
2. Moreover, compared with conventional HACO-OFDM, RHO-OFDM can eliminate error propagation in NOMA-VLC systems, whilst maintaining both high spectral and power efficiency.
3. Thanks to no error propagation, the proposed RHO-OFDM-NOMA achieves better BER performance than HACO-OFDM-NOMA for users with worse channel quality. Moreover, a significantly high data rate is achieved by RHO-OFDM-NOMA compared with the NOMA schemes using conventional O-OFDM.

2. System Model and VLC Channel

2.1. System Model

In the paper, a typical VLC system is considered, in which a single LED-based transmitter installed on the ceiling is used to support the downlink communication, as shown in Figure 1 [28]. On the receiver plane, M users each equipped with a photo-diode (PD) are simultaneously served by the NOMA transmission in the VLC system. The transmitted data for the M users are modulated by the light intensity of LED. The light signal is transformed to an electrical signal by the photodiode of each user, and the direct detection is subsequently performed to extract the transmitted data.

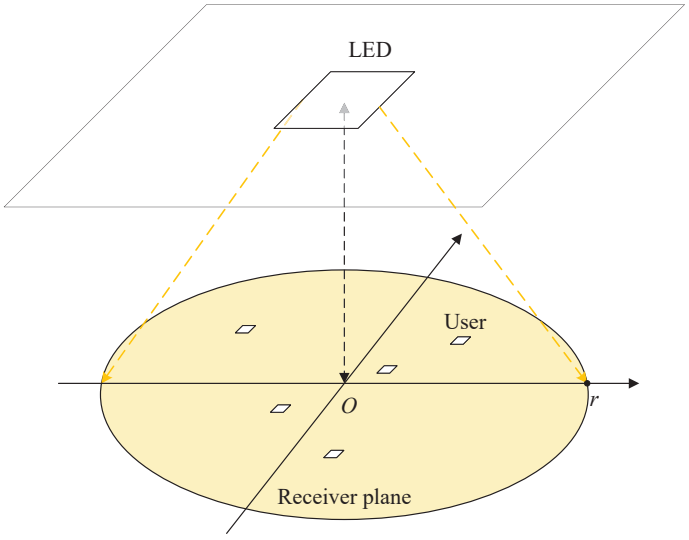

Figure 1. VLC system model.

2.2. VLC Channel

In VLC, the channel attenuation from the LED-based transmitter to the m-th user is given by

$$h_m = \begin{cases} \frac{\rho A_m (d+1)}{2\pi l_m^2} \cos^d(\phi_m) T_s(\psi_m) g(\psi_m) \cos(\psi_m), & 0 \le \psi_m \le \psi_c \\ 0, & \psi_m > \psi_c \end{cases} \quad (1)$$

where $m = 1, 2, \cdots, M$, ρ is the O/E conversion efficiency; l_m denotes the distance from the transmitter to the PD; A_m represents the detector area; d denotes the order of Lambertian emission and is a function of the semi-angle at half power $\Phi_{1/2}$ via $d = -\ln 2/\ln(\cos(\Phi_{1/2}))$; ϕ represents the angle of irradiance; ϕ_m is the angle of incidence; ψ_c is the field of view (FOV) of the receiver; and $T_s(\psi_m)$ denotes the gain of the optical concentrator, which is calculated as

$$g(\psi_m) = \begin{cases} \frac{n_c^2}{\sin^2(\psi_c)}, & 0 \le \psi_m \le \psi_c \\ 0, & \psi_m > \psi_c \end{cases} \tag{2}$$

where n_c is the refractive index. Furthermore, the received signal is contaminated by noise, which can be modeled as the additive Gaussian noise with zero mean and variance of

$$\sigma_m^2 = \sigma_{\text{sh},m}^2 + \sigma_{\text{th},m}^2, \tag{3}$$

Here, σ_m^2 is the variance of the m-th user, $\sigma_{\text{sh},m}^2$ and $\sigma_{\text{th},m}^2$ are the variances of the shot noise and thermal noise, which can be calculated according to [28].

3. Transmitter Design of RHO-OFDM-NOMA

The transmitted symbols of the NOMA users are superimposed in different power levels. Without loss of generality, we sort the M users in ascending order on the basis of channel qualities. In the NOMA system, successive interference cancellation (SIC) is employed to decode the transmitted symbols. To be specific, the m-th user decodes the transmitted symbols of the first $m-1$ users, and subsequently removes the interference of the decoded symbols from the received signal. Furthermore, the symbol of the m-th user can be decoded by treating the transmitted symbols of the remaining $M-m$ users as noise. When HACO-OFDM is directly combined with NOMA, the clipping distortion is determined by the transmitted symbols of all users. However, the users with worse channel qualities can only decode the transmitted symbols of part users. Therefore, the clipping distortion cannot be successfully removed for the users with worse channel quality, leading to unavoidable error propagation.

To address the problem of error propagation, a novel hybrid OFDM scheme, termed RHO-OFDM, is conceived for NOMA-VLC. In the proposed hybrid methodology, different OFDM schemes are adopted for the transmission of the NOMA users according to their channel qualities at the odd-indexed subcarriers. Since the transmitted symbol of the first user can be decoded by all users and consumes most of the transmitted power, the power-efficient ACO-OFDM scheme is adopted for the first user. Let $Q_{m,k}$ denote the QAM symbol loaded at the k-th subcarrier for the m-th user. The frequency-domain signal of the first user is written as

$$X_k = \begin{cases} \sqrt{p_{1,k}} Q_{1,k}, & k = 2i+1, \\ \sqrt{p_{1,k}} Q_{1,N-k}^*, & k = N-(2i+1), \\ 0, & \text{otherwise}, \end{cases} \tag{4}$$

where $i = 0, 1, \cdots, N/4-1$, $p_{1,k}$ is the power allocated to $Q_{1,k}$, and N represents the number of subcarriers. After the IFFT operation is performed on X_k, the signal x_n is obtained as

$$x_n = \frac{1}{\sqrt{N}} \sum_{k=0}^{N-1} X_k e^{j\frac{2\pi nk}{N}}, n = 0, 1, \cdots, N-1. \tag{5}$$

By directly removing the negative part of x_n, the non-negative ACO-OFDM signal can be generated in a power-efficient manner. Furthermore, the transmitted symbols of the remaining users cannot be decoded by all users. Therefore, the clipping-free O-OFDM signal is used for the transmitted symbols of the remaining users, in which the clipping

operation is not used to avoid the clipping distortion. The frequency-domain signal for the remaining users is written as

$$X_k^{\text{free}} = \begin{cases} \sum_{m=2}^{M} \sqrt{p_{m,k}} Q_{m,k}, & k = 2i+1, \\ \sum_{m=2}^{M} \sqrt{p_{m,k}} Q_{m,k}^*, & k = N-(2i+1), \\ 0, & \text{otherwise}, \end{cases} \tag{6}$$

where $p_{m,k}$ denotes the power allocated to $Q_{m,k}$. The time-domain clipping-free signal, denoted by x_n^{free}, is generated through the IFFT operation, which is expressed as

$$x_n^{\text{free}} = \frac{1}{\sqrt{N}} \sum_{k=0}^{N-1} X_k^{\text{free}} e^{j\frac{2\pi nk}{N}}, n = 0, 1, \cdots, N-1. \tag{7}$$

Since the clipping distortion is avoided, the error propagation can be eliminated.

In order to effectively exploit the subcarrier resource, the M NOMA users further share the real parts of the even-indexed subcarriers through PAM-DMT. Let $P_{m,k}$ represent the PAM symbol loaded at the k-th subcarrier for the m-th user. Furthermore, the frequency-domain signal of PAM-DMT-NOMA is expressed as

$$Y_k = \begin{cases} j \sum_{m=1}^{M} \sqrt{p_{m,k}} P_{m,k}, & k = 2q, \\ -j \sum_{m=1}^{M} \sqrt{p_{m,k}} P_{m,k}, & k = N-2q, \\ 0, & \text{otherwise}, \end{cases} \tag{8}$$

where $q = 1, 2, \cdots, N/4-1$. The signal Y_k is input into the IFFT module to yield the signal y_n, given by

$$y_n = \frac{1}{\sqrt{N}} \sum_{k=0}^{N-1} Y_k e^{j\frac{2\pi nk}{N}}, n = 0, 1, \cdots, N-1, \tag{9}$$

which is subsequently clipped for the sake of the non-negativity. Furthermore, the ACO-OFDM, clipping-free O-OFDM, and PAM-DMT signals are superimposed to realize high spectral efficiency, which is given by

$$z_n = \lfloor x_n \rfloor_c + x_n^{\text{free}} + \lfloor y_n \rfloor_c. \tag{10}$$

where $\lfloor \cdot \rfloor_c$ denotes the clipping operation. Note that z_n is bipolar due to the signal component x_n^{free}. Therefore, a reconstruction signal is further introduced to guarantee the non-negativity. In this way, the RHO-OFDM signal is written as

$$z_n^{\text{RHO}} = z_n + b_n, \tag{11}$$

where b_n is the reconstruction signal. For the sake of the non-negativity and no interference with the transmitted symbols, the reconstruction signal can be calculated as

$$b_n = -\min\left\{ z_n, z_{\text{mod}(\frac{N}{2}-n,N)}, z_{\text{mod}(\frac{N}{2}+n,N)}, z_{\text{mod}(N-n,N)} \right\}, \tag{12}$$

where $\min\{\cdot\}$ denotes the minimum of the sequence, and $\text{mod}\{\}$ is the operation for calculating the remainder. It can be proved that the reconstruction signal in (12) can guarantee the non-negativity, and is only loaded at the real part of the even-indexed subcarrier, which implies that no interference is imposed on the transmitted symbols. The detailed proof is provided in Appendix A.

The architecture of the RHO-OFDM-NOMA transmitter is provided in Figure 2. The transmitted symbols of the NOMA users are modulated by ACO-OFDM, the clipping-free

O-OFDM, and PAM-DMT. Subsequently, the three O-OFDM signal components are combined for hybrid transmission, and the reconstruction signal is further added to generate the non-negative RHO-OFDM signal.

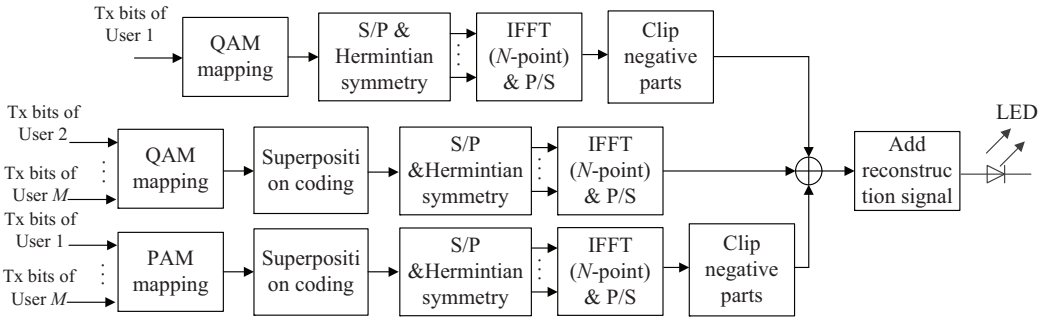

Figure 2. Transmitter architecture of the proposed RHO-OFDM-NOMA.

4. Receiver of RHO-OFDM-NOMA

With the aid of the photodiode, the light signal is detected and converted into the electrical signal at the receiver, which is expressed as

$$z_{m,n} = h_{m,n} * z_n^{\mathrm{RHO}} + w_{m,n}, \tag{13}$$

where $*$ denotes the convolution operation, $h_{m,n}$ is the channel impulse response, and $w_{m,n}$ denotes the noise with variance of σ_m^2. Since the multipath delays are negligible in VLC, $h_{m,n} = h_m \delta(n)$ is considered in the simulation, where $\delta(n)$ is the Dirac Delta function. The received signal is subsequently processed by an FFT block. The frequency-domain signal for the m-th user is given by

$$Z_{m,k} = H_{m,k} Z_k^{\mathrm{RHO}} + W_{m,k}, \tag{14}$$

where $H_{m,k}$, Z_k^{RHO}, and $W_{m,k}$ are the FFT output of $h_{m,n}$, z_n^{RHO}, and $w_{m,n}$, respectively. After one-tap equalization, the equalized signal of $Z_{m,k}$ is written as

$$\widehat{Z}_{m,k} = Z_k^{\mathrm{RHO}} + W_{m,k} / H_{m,k}. \tag{15}$$

Observing the odd-indexed subcarriers that convey the transmitted symbols, we have

$$\widehat{Z}_{m,2i+1} = \sum_{m=1}^{M} \sqrt{p_{m,2i+1}} Q_{m,2i+1} + W_{m,2i+1} / H_{m,2i+1}. \tag{16}$$

The user can decode the transmitted symbol through the SIC process. Furthermore, at the imaginary part of the even-indexed subcarrier, the frequency-domain signal is written as

$$\mathrm{Im}\left\{\widehat{R}_{m,2q}\right\} = \sum_{m=1}^{M} \sqrt{p_{m,2q}} P_{2q} + X_{2q}^{\mathrm{clip}} + \mathrm{Im}\left\{\widehat{W}_{m,2q}\right\}, \tag{17}$$

where X_{2q}^{clip} is the clipping distortion caused by ACO-OFDM, and $\mathrm{Im}\left\{\widehat{R}_{m,2q}\right\}$ and $\mathrm{Im}\left\{\widehat{W}_{m,2q}\right\}$ denote the imaginary part of $\widehat{R}_{m,2q}$ and $\widehat{W}_{m,2q}$, respectively. Note that the clipping distortion is only determined by the transmitted symbol of the first user, which can be decoded by all users. Therefore, the clipping distortion is first regenerated and removed from the received signal $\mathrm{Im}\left\{\widehat{R}_{m,2q}\right\}$ based on the decoded symbol of the first user. Subsequently, the transmitted PAM symbol can be decoded through the SIC process.

The block diagram of the RHO-OFDM-NOMA receiver is provided in Figure 3. By executing the FFT operation on the received signal, the frequency-domain signal is obtained, which can be used to decode the transmitted QAM symbol of the user through the

SIC process. Furthermore, the clipping distortion caused by the ACO-OFDM branch is reproduced and removed from the received signal based on the decoded QAM symbol of the first user. Subsequently, the transmitted PAM symbol of the user can be decoded through the SIC process.

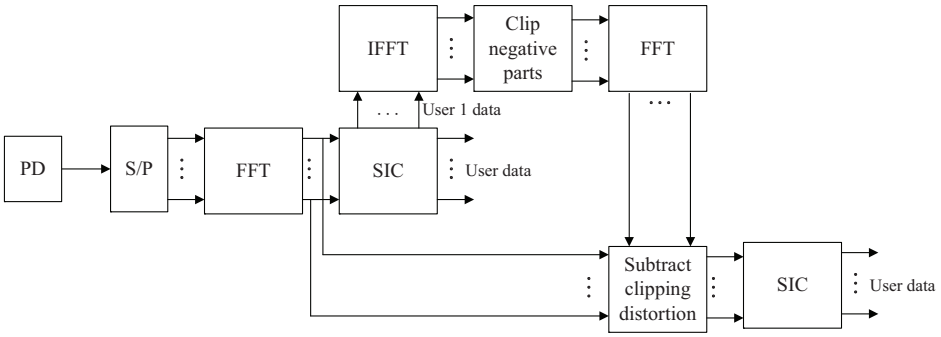

Figure 3. Receiver architecture of the proposed RHO-OFDM-NOMA.

5. Theoretical Performance Analysis

5.1. Sum Rate of RHO-OFDM-NOMA

The sum rate of the proposed RHO-OFDM-NOMA is theoretically analyzed. Since the m-th user can decode the transmitted symbols of the first $m-1$ users and treat the remaining ones as noise, the signal to interference plus noise ratio (SINR) for the m-th user at the $(2i+1)$-th subcarrier is computed as

$$\mathrm{SINR}_{m,2i+1} = \frac{p_{m,2i+1}}{\sum\limits_{l=m+1}^{M} p_{l,2i+1} + \sigma_m^2 / H_{m,2i+1}^2}. \tag{18}$$

In RHO-OFDM-NOMA, the clipping distortion is only determined by the transmitted symbol of first user, which can be decoded by all users according to the principle of NOMA. On the other hand, when the transmitted symbols of all users are modulated by ACO-OFDM in HACO-OFDM, the clipping distortion is determined by all users. Therefore, in order to successfully eliminate the clipping distortion, the user is required to decode the transmitted symbols of all users, which restricts the data rate to the minimum one of all users. By contrast, the proposed RHO-OFDM-NOMA removes the restriction on the data rate by the well-designed hybrid transmission architecture. In this way, the data rate of the $(2i+1)$-th subcarrier achieved by the m-th user in RHO-OFDM-NOMA can be computed as

$$\begin{aligned} R_{m,2i+1} &= \log_2(1 + \mathrm{SINR}_{2i+1}) \\ &= \log_2\left(1 + \frac{p_{m,2i+1}}{\sum\limits_{l=m+1}^{M} p_{l,2i+1} + \sigma_m^2 / H_{m,2i+1}^2}\right). \end{aligned} \tag{19}$$

Furthermore, the SINR for the m-th user at the imaginary part of the $2q$-th subcarrier is expressed as

$$\mathrm{SINR}_{m,2q} = \frac{p_{m,2q}}{\sum\limits_{l=m+1}^{M} p_{l,2q} + \sigma_m^2 / H_{m,2q}^2}. \tag{20}$$

Therefore, the data rate at the imaginary part of the $2q$-th subcarrier is given by

$$\begin{aligned} R_{m,2q} =& \log_2\left(1+\mathrm{SINR}_{m,2q}\right) \\ =& \log_2\left(1+\frac{p_{m,2q}}{\sum\limits_{l=m+1}^{M} p_{l,2q}+\sigma^2_{m,2q}/\left(2H^2_{m,2q}\right)}\right). \end{aligned} \tag{21}$$

The sum rate achieved by RHO-OFDM-NOMA is expressed as

$$R_{\mathrm{sum}} = \sum_{m=1}^{M}\sum_{i=0}^{N/4-1} R_{m,2i+1} + \sum_{m=1}^{M}\sum_{q=1}^{N/4-1} R_{m,2q}. \tag{22}$$

5.2. Complexity Analysis

The complexity of the OFDM-based system is dominated by IFFT/FFT, while the complexity of other operations can be negligible [21]. Therefore, the computational complexity of the IFFT/FFT operations is analyzed to characterize the complexity of the proposed scheme. When the radix-2 algorithm is adopted, we can use $2\mathcal{O}(N\log_2 N)$ to characterize the computational complexity of the N-point IFFT/FFT operation executed on the complex-valued frame.

At the transmitter, three IFFT operations are required in RHO-OFDM-NOMA. To expound further, the ACO-OFDM and clipping-free O-OFDM signals exploit one IFFT operation performed on the complex-valued QAM symbols, respectively. Since only the odd-indexed subcarriers are used, half of the computational complexity can be reduced. Therefore, the computational complexity of ACO-OFDM and clipping-free O-OFDM can be characterized as $\mathcal{O}(N\log_2 N)$. Additionally, one IFFT operation performed on the imaginary-valued PAM symbols is required in PAM-DMT, which leads to $\frac{1}{2}\mathcal{O}(N\log_2 N)$ since only even-indexed subcarriers are used. Therefore, the total computational complexity of the RHO-OFDM-NOMA transmitter is $\frac{5}{2}\mathcal{O}(N\log_2 N)$, which is relatively higher than that of the HACO-OFDM-NOMA transmitter, i.e., $\frac{3}{2}\mathcal{O}(N\log_2 N)$. Nevertheless, the increased complexity of the RHO-OFDM-NOMA transmitter is not a problem since the transmitter generally possesses strong ability on signal processing.

At the receiver, the proposed RHO-OFDM-NOMA uses the same detection process as HACO-OFDM-NOMA, in which two FFT operations and one IFFT operation are required. The two FFT operations are performed on the real-valued frame, leading to the total complexity of $2\mathcal{O}(N\log_2 N)$. Additionally, due to the complex-valued frame, the IFFT operation has the complexity of $\mathcal{O}(N\log_2 N)$. Therefore, the total complexity of the RHO-OFDM-NOMA receiver is $\mathcal{O}(N\log_2 N)$, which is the same as that of the HACO-OFDM-NOMA receiver.

6. Simulation Results and Discussion

Simulations are performed to characterize the performance of different NOMA schemes. In the simulation, one LED array installed on the ceiling is used as a transmitter, which simultaneously serves two users distributed on the receiver plane. The receiver plane is located 2 m away from the ceiling. The relevant system parameters are summarized in Table 1 [29,30].

Table 1. Parameters of the LED and receiver in NOMA-VLC.

Parameter	Value	Parameter	Value
Field of view of the receiver	80 (deg.)	Detector area	1 (cm^2)
Gain of the optical concentrator	1.0	Refractive index	1.5
O/E conversion efficiency	0.23 (A/W)	Communication bandwidth	100 (MHz)
Number of LEDs per array	60×60	LED interval	0.01 (m)
Semi-angle at half power	70 (deg.)		

The BER curves of two users in the hybrid OFDM-NOMA system are illustrated in Figures 4 and 5, respectively. In the simulation, 64-QAM and 8-PAM are adopted, and two scenarios are considered. In Scenario 1, the locations of the two users are $(3.0, 2.9)$ and $(0.8, 0.1)$, respectively. In Scenario 2, the locations of the two users are $(3.3, 3.3)$ and $(-1.3, -1.3)$, respectively. The two users in Scenario 1 are located close to each other while the users are located far from each other in Scenario 2. In both scenarios, User 1 has worse channel quality than User 2 since it is located farther from the LED array. Therefore, most of the power is allocated to User 1 according to the philosophy of NOMA. In the simulation, the proportion of the power of User 1 is set to 99.5%.

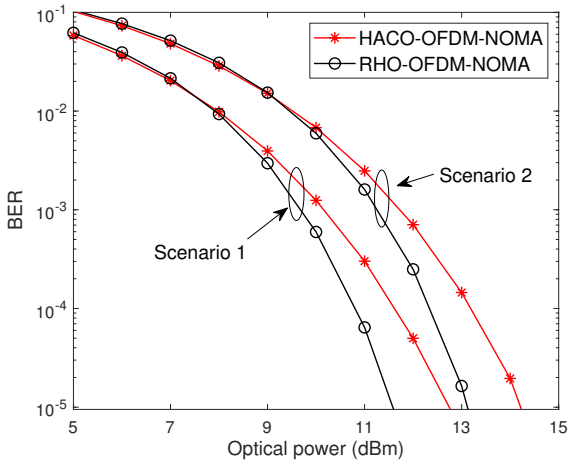

Figure 4. BER performance of User 1 using HACO-OFDM and RHO-OFDM-NOMA.

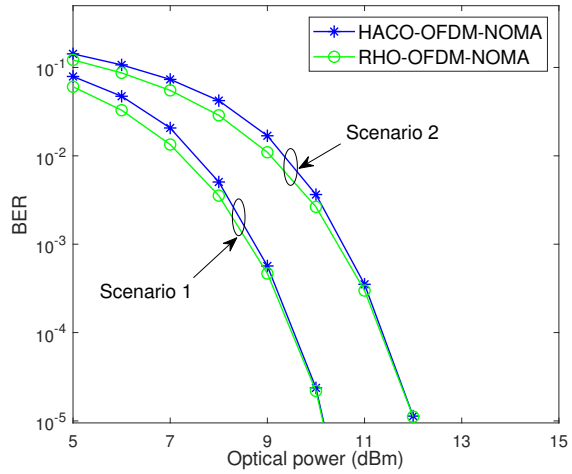

Figure 5. BER performance of User 2 using HACO-OFDM and RHO-OFDM-NOMA.

In the NOMA-based system, successive interference cancellation (SIC) is employed for NOMA users at the receiver. Since the first user has worse channel quality, the first user can only decode its own transmitted symbol, and the transmitted symbol of User 2

is treated as noise. However, when HACO-OFDM is directly combined with NOMA, the clipping noise is determined by the transmitted symbols of all users [18]. Therefore, the clipping distortion cannot be successfully regenerated and eliminated for User 1, leading to error propagation. By contrast, the error propagation can be eliminated in the proposed RHO-OFDM-NOMA. Therefore, it is observed from Figure 4 that RHO-OFDM-NOMA achieves better BER performance than HACO-OFDM-NOMA for User 1. On the other hand, User 2 can decode the transmitted symbols of two users. Therefore, the clipping distortion can be eliminated in HACO-OFDM-NOMA. Meanwhile, in contrast to HACO-OFDM, the reconstruction process is introduced to guarantee the non-negativity. It is clearly seen from Figure 5 that HACO-OFDM-NOMA and RHO-OFDM-NOMA achieve similar BER performance for User 2, which implies that the proposed RHO-OFDM still has the superiority of high power efficiency, regardless of using the reconstruction process or not.

Furthermore, the sum rates of RHO-NOMA-VLC for Scenario 1 and Scenario 2 are illustrated in Figures 6 and 7, respectively. The sum rates of HACO-OFDM-NOMA, DCO-OFDM-NOMA, and ACO-OFDM-NOMA are provided for comparison [26,31]. The DC bias of 10 dB is taken into consideration in DCO-OFDM-NOMA. Compared with conventional DCO-OFDM-NOMA and ACO-OFDM-NOMA, the proposed RHO-OFDM-NOMA has the advantage of high power efficiency, whist improving spectral efficiency. Meanwhile, the error propagation in HACO-OFDM-NOMA induces the sum rate reduction. Therefore, it is seen from Figures 6 and 7 that the proposed RHO-OFDM-NOMA substantially outperforms other NOMA schemes in terms of the sum rate.

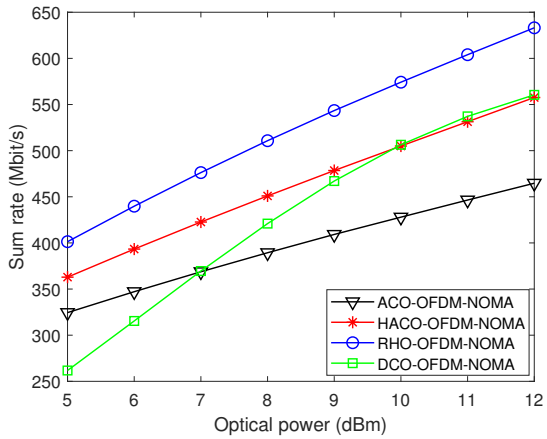

Figure 6. Sum rate of the NOMA-VLC system using different OFDM schemes for Scenario 1.

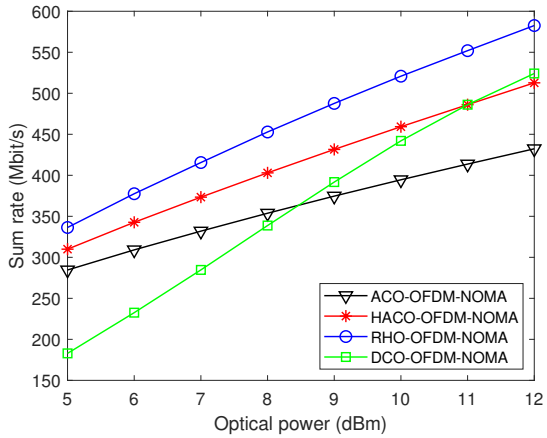

Figure 7. Sum rate of the NOMA-VLC system using different OFDM schemes for Scenario 2.

In order to make a comprehensive evaluation, the average sum rate of different OFDM-NOMA schemes for VLC system are provided in Figure 8. A circular VLC cell with a radius

of $r = 3$ m is considered. The average sum rate is obtained by assuming that the two users are uniformly distributed in the VLC cell. It is seen from Figure 8 that the performance of RHO-OFDM-NOMA is much better than that of the conventional scheme. Furthermore, the spectral efficiency is defined as the ratio of the data rate to the bandwidth. Since the same bandwidth is adopted for different schemes, the higher data rate indicates higher spectral efficiency. Therefore, the proposed RHO-OFDM-NOMA has higher spectral efficiency than other schemes, which makes it a competitive transmission scheme for multiuser VLC.

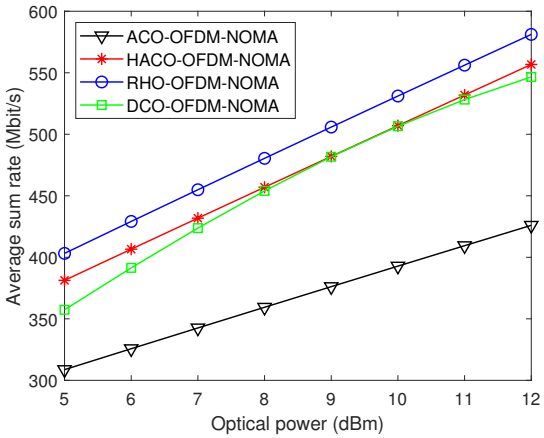

Figure 8. Average sum rate of the NOMA-VLC system using different OFDM schemes.

7. Conclusions

A novel RHO-OFDM-NOMA is conceived for VLC in this paper. In RHO-OFDM-NOMA, ACO-OFDM and clipping-free O-OFDM are used for different users based on their channel qualities, which are further combined with PAM-DMT to enhance the spectral efficiency. The well-designed hybrid transmission architecture in RHO-OFDM-NOMA can eliminate the error propagation that arises in the NOMA-VLC system using conventional hybrid O-OFDM. Owing to having no error propagation, the proposed RHO-OFDM-NOMA can support better BER performance compared with HACO-OFDM-NOMA for the users with worse channel quality. Moreover, a much higher data rate is obtained by RHO-OFDM-NOMA than the NOMA schemes using DCO-OFDM and ACO-OFDM, which makes it a prospective technology of the multiuser transmission for VLC.

Author Contributions: Conceptualization, B.L. and S.F.; methodology, B.L.; software, J.S.; validation, B.L., J.S., and S.F.; formal analysis, B.L.; investigation, J.S.; resources, B.L.; data curation, J.S.; writing—original draft preparation, B.L.; writing—review and editing, J.S.; visualization, J.S.; supervision, S.F.; project administration, S.F.; funding acquisition, S.F. All authors have read and agreed to the published version of the manuscript.

Funding: This research was funded by the National Natural Science Foundation of China under Grants 62001219, 62201275 and 62201274, the Natural Science Foundation of Jiangsu Province under Grants BK20190582 and BK20210641, the open research fund of National Mobile Communications Research Laboratory, Southeast University under Grant 2021D11, and the Startup Foundation for Introducing Talent of NUIST.

Institutional Review Board Statement: Not applicable.

Informed Consent Statement: Not applicable.

Data Availability Statement: The data that support the findings of this study are available from the corresponding author upon reasonable request.

Conflicts of Interest: The authors declare no conflict of interest.

Appendix A

We first prove that the reconstruction signal in (12) can generate the non-negative RHO-OFDM signal. Based on (12), the following inequality holds:

$$z_n \geq \min\left\{z_n, z_{\mathrm{mod}(\frac{N}{2}-n,N)}, z_{\mathrm{mod}(\frac{N}{2}+n,N)}, z_{\mathrm{mod}(N-n,N)}\right\}. \tag{A1}$$

Therefore, we have

$$z_n^{\mathrm{RHO}} = z_n + b_n = z_n - \min\left\{z_n, z_{\mathrm{mod}(\frac{N}{2}-n,n)}, z_{\mathrm{mod}(\frac{N}{2}+n,n)}, z_{\mathrm{mod}(N-n,n)}\right\} \geq 0. \tag{A2}$$

It is observed that the introduced reconstruction signal can make the RHO-OFDM signal non-negative.

Furthermore, we will prove that the reconstruction signal is loaded at the real part of the even-indexed subcarrier. According to (12), the reconstruction signal has the following characteristics:

$$\begin{cases} b_n = b_{n+\frac{N}{2}}, & n = 0, \frac{N}{4}, \\ b_n = b_{\frac{N}{2}-n} = b_{n+\frac{N}{2}} = b_{N-n}, & n = 1, 2, \cdots, \frac{N}{4}-1. \end{cases} \tag{A3}$$

By performing FFT operation on b_n, we have

$$\begin{aligned} B_k =& \frac{1}{\sqrt{N}} \sum_{n=0}^{N-1} b_n e^{-j\frac{2\pi nk}{N}} = \frac{1}{\sqrt{N}} \sum_{n=1}^{\frac{N}{4}-1} b_n \left(e^{-j\frac{2\pi nk}{N}} + e^{-j\pi k + j\frac{2\pi nk}{N}} + e^{-j\frac{2\pi nk}{N} - j\pi k} + e^{j\frac{2\pi nk}{N}}\right) \\ &+ \frac{1}{\sqrt{N}} \left[b_0 \left(1 + e^{-j\pi k}\right) + b_{\frac{N}{4}} e^{-j\frac{\pi}{2}k} \left(1 + e^{-j\pi k}\right)\right] \\ =& \frac{1}{\sqrt{N}} \sum_{n=1}^{\frac{N}{4}-1} b_n \left(e^{-j\frac{2\pi nk}{N}} + e^{j\frac{2\pi nk}{N}}\right) \left(1 + e^{-j\pi k}\right) + \frac{1}{\sqrt{N}} \left(b_0 + b_{\frac{N}{4}} e^{-j\frac{\pi}{2}k}\right) \left(1 + e^{-j\pi k}\right) \\ =& \frac{1}{\sqrt{N}} \sum_{n=1}^{\frac{N}{4}-1} 2b_n \cos\left(\frac{2\pi nk}{N}\right) \left(1 + e^{-j\pi k}\right) + \frac{1}{\sqrt{N}} \left(b_0 + b_{\frac{N}{4}} e^{-j\frac{\pi}{2}k}\right) \left(1 + e^{-j\pi k}\right) \end{aligned} \tag{A4}$$

For the odd-indexed subcarrier, i.e., $k = 2i + 1$, we have

$$1 + e^{-j\pi k} = 1 + e^{-j2\pi i - j\pi} = 0. \tag{A5}$$

Therefore, B_k at the odd-indexed subcarrier is calculated as

$$B_k = 0, \; k = 2i + 1, \tag{A6}$$

which implies that the reconstruction signal does not induce any interference with the transmitted symbol at the odd-indexed subcarrier. Furthermore, for the even-indexed subcarrier, i.e., $k = 2q$, we have

$$1 + e^{-j\pi k} = 2, \; 1 + e^{-j\frac{\pi}{2}k} = (-1)^q. \tag{A7}$$

Therefore, B_k at the even-indexed subcarrier is written as

$$B_k = \frac{1}{\sqrt{N}} \sum_{n=1}^{\frac{N}{4}-1} 4b_n \cos\left(\frac{2\pi nk}{N}\right) + \frac{2}{\sqrt{N}} \left[b_0 + (-1)^q b_{\frac{N}{4}}\right], \; k = 2q. \tag{A8}$$

It is found that B_k is real for $k = 2q$, which indicates that the reconstruction signal is only loaded at the real parts of the even-indexed subcarrier. Hence, the introduced reconstruction signal does not contaminate the QAM and PAM symbols at the corresponding subcarriers.

References

1. Shi, J.; Niu, W.; Ha, Y.; Xu, Z.; Li, Z.; Yu, S.; Chi, N. AI-enabled intelligent visible light communications: Challenges, progress, and future. *Photonics* **2022**, *9*, 529. [CrossRef]
2. Abdelhady, A.M.; Amin, O.; Salem, A.K.S.; Alouini, M.-S.; Shihada, B. Channel characterization of IRS-based visible light communication systems. *IEEE Trans. Commun.* **2022**, *70*, 1913–1926.
3. Ndjiongue, A.R.; Ngatched, T.M.N.; Dobre O.A.; Armada, A.G. VLC-based networking: Feasibility and challenges. *IEEE Netw.* **2020**, *34*, 158–165. [CrossRef]
4. Wang, J.; Ge, H.; Lin, M.; Wang, J.; Dai, J.; Alouini, M.S. On the secrecy rate of spatial modulation-based indoor visible light communications. *IEEE J. Sel. Areas Commun.* **2019**, *37*, 2087–2101. [CrossRef]
5. Liu, Y.; Mu, X.; Liu, X.; Renzo, M.D.; Ding, Z.; Schober, R. Reconfigurable intelligent surface-aided multi-user networks: Interplay between NOMA and RIS. *IEEE Wireless Commun.* **2022**, *29*, 169–176.
6. Arfaoui, M.A.; Ghrayeb, A.; Assi, C.; Qaraqe, M. CoMP-assisted NOMA and cooperative NOMA in indoor VLC cellular systems. *IEEE Trans. Commun.* **2022**, *70*, 6020–6034. [CrossRef]
7. Marshoud, H.; Muhaidat, S.; Sofotasios, P.C.; Hussain, S.; Imran, M.A.; Sharif, B.S. Optical non-orthogonal multiple access for visible light communication. *IEEE Wireless Commun.* **2018**, *25*, 82–88. [CrossRef]
8. Liu, Y.; Qin, Z.; Elkashlan, M.; Ding, Z.; Nallanathan A.; Hanzo, L. Nonorthogonal multiple access for 5G and beyond. *Proc. IEEE* **2017**, *105*, 2347–2381.
9. Obeed, M.; Salhab, A.M.; Alouini M.-S.;Zummo, S.A. On optimizing VLC networks for downlink multi-user transmission: A survey. *IEEE Commun. Surveys Tuts.* **2019**, *21*, 2947–2976.
10. Xu, W.; Li, X.; Lee, C.-H.; Pan M.; Feng, Z. Joint sensing duration adaptation, user matching, and power allocation for cognitive OFDM-NOMA systems. *IEEE Trans. Wireless Commun.* **2018**, *17*, 1269–1282. [CrossRef]
11. Hong, H.; Li, Z. Hybrid adaptive bias OFDM-based IM/DD visible light communication system. *Photonics* **2021**, *8*, 257.
12. Cao, B.; Yuan, K.; Li, H.; Duan, S.; Li, Y.; Ouyang, Y. The performance improvement of VLC-OFDM system based on reservoir computing. *Photonics* **2022**, *9*, 185. [CrossRef]
13. Carruthers, J.B.; Kahn, J.M. Multiple-subcarrier modulation for nondirected wireless infrared communication. *IEEE J. Sel. Areas Commun.* **1996**, *14*, 538–546.
14. Armstrong, J.; Lowery, A.J. Power efficient optical OFDM. *Electron. Lett.* **2006**, *42*, 370–372. [CrossRef]
15. Lee, S.; Randel, S.; Breyer, F.; Koonen, A. PAM-DMT for intensity-modulated and direct-detection optical communication systems. *IEEE Photon. J.* **2009**, *21*, 1749–1751.
16. Dissanayake, S.D.; Armstrong, J. Comparison of ACO-OFDM, DCO-OFDM and ADO-OFDM in IM/DD systems. *J. Lightw. Technol.* **2013**, *31*, 1063–1072.
17. Zhang, X.; Babar, Z.; Petropoulos, P.; Haas, H.; Hanzo, L. The evolution of optical OFDM. *IEEE Commun. Surveys Tuts.* **2021**, *23*, 1430–1457. [CrossRef]
18. Ranjha, B.; Kavehrad, M. Hybrid asymmetrically clipped OFDM based IM/DD optical wireless system. *J. Opt. Commun. Netw.* **2014**, *6*, 387–396. [CrossRef]
19. Li, B.; Xu, W.; Zhang, H.; Zhao, C.; Hanzo, L. PAPR reduction for hybrid ACO-OFDM aided IM/DD optical wireless vehicular communications. *IEEE Trans. Veh. Technol.* **2017**, *66*, 9561–9566. [CrossRef]
20. Yang, F.; Gao, J. Dimming control scheme with high power and spectrum efficiency for visible light communications. *IEEE Photon. J.* **2017**, *9*, 1–13.
21. Hu, W.-W. Design of cyclic shifted PAM-DMT signals in HACO-OFDM visible light communication. *IEEE Commun. Lett.* **2020**, *24*, 2834–2838.
22. Wang, Q.; Wang, Z.; Dai, L. Asymmetrical hybrid optical OFDM for visible light communications with dimming control. *IEEE Photon. Technol. Lett.* **2015**, *27*, 974–977. [CrossRef]
23. Chen, C.; Zhong, W.; Yang, H.; Du, P. On the performance of MIMO-NOMA-based visible light communication systems. *IEEE Photon. Technol. Lett.* **2017**, *30*, 307–310. [CrossRef]
24. Shi, J.; Hong, Y.; Deng, R.; He, J.; Chen, L.-K.; Chang, G.-K. Demonstration of real-time software reconfigurable dynamic power-and-subcarrier allocation scheme for OFDM-NOMA-based multi-user visible light communications. *J. Lightw. Technol.* **2019**, *37*, 4401–4409. [CrossRef]
25. Shi, J.; He, J.; Wu, K.; Ma, J. Enhanced performance of asynchronous multi-cell VLC system using OQAM/OFDM-NOMA. *J. Lightw. Technol.* **2019**, *37*, 5212-5220.
26. Wang, G.; Shao, Y.; Chen, L. -K.; Zhao, J. Subcarrier and power allocation in OFDM-NOMA VLC systems. *IEEE Photon. Technol. Lett.* **2021**, *33*, 189–192.
27. Jiang, R.; Sun, C.; Tang, X.; Zhang, L.; Wang, H.; Zhang, A. Joint user-subcarrier pairing and power allocation for uplink ACO-OFDM-NOMA underwater visible light communication systems. *J. Lightw. Technol.* **2020**, *39*, 1997–2007.
28. Marshoud, H.; Sofotasios, P.C.; Muhaidat, S.; Karagiannidis, G.K.; Sharif, S.B. On the performance of visible light communication systems with non-orthogonal multiple access. *IEEE Trans. Wireless Commun.* **2017**, *16*, 6350–6364. [CrossRef]

29. Li, B.; Wang, J.; Zhang, R.; Shen, H.; Zhao, C.; Hanzo, L. Multiuser MISO transceiver design for indoor downlink visible light communication under per-LED optical power constraints. *IEEE Photon. J.* **2015**, *7*, 1–13.
30. Komine, T.; Nakagawa, M. Fundamental analysis for visible-light communication system using LED lights. *IEEE Trans. Consum. Electron.* **2004**, *50*, 100–107.
31. Jayashree, P.; Holey, P.; Kappala, V.K.; Das, S.K. Performance analysis of ACO-OFDM NOMA for VLC communication. *Opt. Quant. Electron.* **2022**, *54*, 1–16.